ISSN 1068-3356, Bulletin of the Lebedev Physics Institute, 2024, Vol. 51, Suppl. 1, pp. S16–S27. © Allerton Press, Inc., 2024.
Russian Text © The Author(s), 2023, published in Kvantovaya Elektronika, 2023, Vol. 53, No. 9, pp. 695–703.

INTERACTION OF LASER RADIATION ON MATTER. LASER PLASMA

Effect of Ion Motion on Generation and Lifetime of Magnetic Fields in a Cluster Plasma Irradiated with Intense Circularly Polarized Laser Pulses

A. A. Andreev[a,b,*], K. Yu. Platonov[c,], and L. A. Litvinov[a]**

[a] *Faculty of Physics, St. Petersburg University, St. Petersburg, 190034 Russia*

[b] *Ioffe Institute, St. Petersburg, 194021 Russia*

[c] *Peter the Great St. Petersburg Polytechnic University, St. Petersburg, 195251 Russia*

**e-mail: alexanderandreev72@yahoo.com*

***e-mail: konstantin_platonov@yahoo.com*

Received October 18, 2023; revised November 15, 2023; accepted November 15, 2023

Abstract—We report a numerical and analytical investigation of the effect of ion motion on the temporal dynamics of a strong quasi-stationary magnetic field arising when submicron clusters are irradiated with circularly polarized radiation. A region of high-density magnetized ions is shown to appear in the central region of the cluster. This region has an increased lifetime compared to that of a cluster without a magnetic field. The presence of a magnetized region leads to a characteristic two-peak dependence of the magnetic field on time.

Keywords: circularly polarized laser pulse, laser cluster plasma, strong quasi-stationary magnetic field

DOI: 10.3103/S1068335624600141

1. INTRODUCTION

As is known [1–4], interaction of an intense short laser pulse with clusters has become an important area of research. The studies are important for the practical use of laser cluster plasma [5]. The authors of a series of works [6–9] showed that a circularly polarized laser pulse of relativistic intensity generates an intense circular current in clusters with a radius of tens and hundreds of nanometers, which leads to the emergence of a quasi-stationary (compared to the laser period duration) magnetic field and transforms the cluster into a magnetic dipole. Preliminary estimates and numerical simulation of the magnetic field of a cluster plasma, published in [7], demonstrate that the quasi-stationary magnetic field strength of a cluster can exceed the field strength of a laser wave and increases with increasing laser pulse intensity and duration. At the same time, an increase in intensity is limited due to the Coulomb explosion (detachment of electrons) of the cluster, and an increase in duration is limited by the time of cluster expansion. Thus, there are optimal laser parameters that make it possible to obtain a maximum possible magnetic field for a given size and material of clusters. Estimates and 3D particle-in-cell (PIC) simulation show [8] that the volumetric energy density of the magnetic field at the cluster center in the optimal case exceeds the volumetric thermal energy density of hot electrons. As a result, the cluster expansion transverse to the magnetic field slows down, and ion dynamics turns out to be related to the time evolution of the magnetic field. As follows from [6], at lower laser intensities the magnetic field has little effect on the motion of ions (the ion gyroradius exceeds the cluster radius), and the cluster expansion (its lifetime) corresponds to the standard model of adiabatic expansion of a hot plasma ball [10] or (for small radii) of the Coulomb expansion of a charged ball [11].

In this work, we study numerically and analytically the case of maximum possible experimentally achievable laser intensities, when not only the electronic but also the ion subsystem of the cluster turns out to be magnetized, the cluster lifetime increases compared to the standard model of thermal expansion, and the dynamics of the magnetic field and the dynamics of the ions turn out to be related.

2. DYNAMICS OF ELECTRONS IN A LASER CLUSTER PLASMA

Intense circularly polarized laser radiation interacting with a cluster plasma generates a longitudinal (along the laser beam axis) quasi-stationary magnetic field (see, for example, [6]). Full-scale 3D PIC calculations of the spatial distribution of the electric field [7, 8], simplified according to the Mie theory [12], show that when a circularly polarized wave is diffracted on a cluster with a diameter of hundreds of nanometers, two regions of concentrated electric field lines are formed on the cluster surface (two "spots" with an enhanced field). In one of the spots, the radial component of the field is directed in such a way that it results in an intense emission of electrons. This electron generation spot rotates around the cluster together with the electric field of a circularly polarized wave, as a result of which, after several revolutions (laser periods), a closed azimuthal current of hot electrons appears around the cluster, generating a longitudinal (along the x axis of the laser beam) magnetic field whose strength is comparable or even exceeds the laser field strength. The density of hot electrons during the laser pulse action is azimuthally inhomogeneous; i.e., opposite the lasing spot, the density is increased, and, in addition to the quasi-uniform electron cloud, a local electron bunch rotating around the cluster is formed. With the end of the laser action, this bunch is isotropicized and expanded, azimuthal inhomogeneities are smoothed out, and an equilibrium axisymmetric distribution of electron density is established. In [8], the dynamics of the electron shell of a cluster (electron orbital parameters) are studied in more detail and, in particular, the amplitude of the magnetic field H is determined:

$$\frac{H}{E_{\text{las}}} \approx \eta a(1+a^2)^{-1/2}\frac{c\tau_{\text{las}}}{4R}. \tag{1}$$

Here, η is the absorption coefficient, τ_{las} is the laser pulse duration, R is the cluster radius, $a = eE_{\text{las}}/(m_e\omega c)$ is the dimensionless amplitude of the laser field E_{las}, m_e is the electron mass, ω is the laser frequency, and c is the speed of light. When the cluster expands (expands after the laser pulse is terminated), its total mechanical (and magnetic) moment is an adiabatic invariant, and the magnetization decreases with increasing cluster volume. Accordingly, for the law of magnetic field decay with time $H(t)$ we can write a simple estimate, in which $H(0) \equiv H(t=0)$ is determined by formula (1):

$$H(t) = H(0)\left[\frac{R(0)}{R(t)}\right]^3. \tag{2}$$

The law of field decay (2) is confirmed by numerical simulation data [8].

3. DYNAMICS OF IONS IN A LASER CLUSTER PLASMA

Let us consider the motion of ions and take into account the resulting distributions of fields and electrons under the action of a laser pulse. Due to their large mass, ions are shifted over significant distances (comparable to the initial radius) at times longer than the characteristic times of electron motion (the time of revolution of an electron around a cluster). The time-averaged quasi-equilibrium state of hot electrons with temperature T_{eh} is described by the Boltzmann distribution

$$n_e(\mathbf{r}) = Zn_{\text{i}}\exp\left[e\varphi(\mathbf{r}) - \frac{\sqrt{m_e^2c^4 + e^2\langle\mathbf{A}^2(\mathbf{r},t)\rangle_t}}{T_{\text{eh}}}\right]$$

in the scalar potential $\varphi(\mathbf{r})$ of the ambipolar field of electrons and ions and in the time-average (over the laser period) vector potential of the transverse field in the cluster zone

$$\mathbf{A}(\mathbf{r},t) = a\frac{m_ec^2}{e}\exp\left(-\frac{t^2}{\tau_{\text{las}}^2}\right)$$
$$\times\left[\mathbf{e}_y\cos\left(\omega\left(t-\frac{x}{c}\right)\right) + \mathbf{e}_z\sin\left(\omega\left(t-\frac{x}{c}\right)\right)\right] + \mathbf{A}_{\text{sc}}(\mathbf{r},t).$$

The vector potential $\mathbf{A}_{\text{sc}}(\mathbf{r}, t)$ describes the cluster-scattered field considered in [12]. Accordingly, the force acting on the ion from the ambipolar field of hot electrons,

$$Ze\mathbf{E} = -Ze\frac{\partial\varphi(\mathbf{r})}{\partial\mathbf{r}} = -\frac{ZT_{\text{eh}}}{n_e(\mathbf{r})}\frac{\partial n_e(\mathbf{r})}{\partial\mathbf{r}} - \frac{Z\partial\sqrt{m_e^2c^4 + e^2\langle\mathbf{A}^2(\mathbf{r},t)\rangle_t}}{\partial\mathbf{r}},$$

is determined by the pressure gradient $n_e T_{eh}$ of hot electrons and the gradient of the time-averaged ponderomotive potential of the transverse field (ponderomotive pressure force [13]). In addition to the ambipolar field of hot electrons, the ions are affected by the force of Coulomb repulsion, which arises due to the uncompensated positive charge of the cluster

$$Q = \int_0^{R(t)} [Zn_i(\mathbf{r}) - n_e(\mathbf{r})]\mathrm{d}V$$

(some electrons are removed by the laser field). Finally, the Lorentz force of the magnetic field (1) also acts on the ions. As a result, when dissipation (terms with viscosity) is neglected, the system of hydrodynamic equations for the motion of cluster ions has the form [9]

$$\frac{\partial v_i}{\partial t} + \frac{v_i \partial}{\partial \mathbf{r}} v_i = -\frac{Z}{m_i}\frac{\partial \sqrt{m_e^2 c^4 + e^2 \langle \mathbf{A}^2(\mathbf{r},t)\rangle_t}}{\partial \mathbf{r}} - \frac{T_{eh}}{m_i n_i}\frac{\partial}{\partial \mathbf{r}}(n_e(\mathbf{r})) - \Omega(t) v_i + \frac{ZeQ\mathbf{r}}{m_i R^3(t)}, \tag{3}$$

$$\left(\frac{\partial}{\partial t} + v_i \frac{\partial}{\partial \mathbf{r}}\right) n_i = -n_i \frac{\partial v_i}{\partial \mathbf{r}}, \tag{4}$$

where $\mathbf{\Omega} = Ze\mathbf{H}(t)/(m_i c)$ is the Larmor frequency of the ion and $\mathbf{H}(t)$ is determined from (2). Note that the hydrodynamic method of describing the motion of ions using Eqs. (3) and (4) assumes a small spread of particle velocities relative to the average (hydrodynamic) value and the absence of multi-flow (different velocities for the same coordinate) currents. From the phase diagrams of ion motion (see Figs. 5b and 5c) it is clear that in the outer regions of the cluster, where a spiral-shaped density structure is formed, there is no multi-flow, and the spread of velocities is small; therefore, the hydrodynamic method used to describe the motion of ions is correct. The electron concentration in (3) consists of two terms, $n_e(r) = n_{0e}(r) + \delta_{n\mathrm{bunch}}(r)\exp[-(\alpha - \omega t)2/\delta\alpha^2]$, corresponding to the spherically symmetric part $n_{0e}(r)$ and the bunch with angular size $\delta\alpha$ (α is the azimuthal angle in the yz plane perpendicular to the x axis of the laser pulse). The term $\sim\delta n_{\mathrm{bunch}}$ is small ($\delta n_{\mathrm{bunch}} \ll n_{0e}$) and can be taken into account using perturbation theory [14]. Note that estimates of the scale of the skin layer in a cluster with ultrarelativistic electrons yield the skin layer length comparable to the cluster radius. For example, for the Au^{+30} cluster with a radius of 100 nm considered below, the length of the skin layer at a laser intensity of 5×10^{22} W/cm^2 is ~40 nm. As a result, there is no significant screening of the laser field, and the expression for the ponderomotive pressure force in (3) includes the vacuum strength of the laser wave field.

Let us analyze the solutions of Eqs. (3) and (4). At low laser intensities ($\alpha \ll 10^2$), the term with the magnetic field is small [the ion gyroradius is much larger than the cluster radius $R(t)$]. The expansion (scatter) of cluster ions after the laser pulse action is related in this limiting case to its heating and Coulomb explosion, which arose due to the partial removal of electrons with charge Q [15]. Thermal expansion has a rate $v_s \approx \sqrt{ZT_{eh}/m_i}$, where the temperature of hot electrons in the field of a circularly polarized wave is estimated as $T_{eh} \approx m_e c^2(\sqrt{1+a^2} - 1)$. The predominance of the thermal or Coulomb expansion mechanism depends on the ratio between the thermal (ZT_{eh}) and Coulomb [$ZeQ/R(0)$] energies of the cluster ion. The dependence of the cluster parameters on time for these two expansion mechanisms can be assessed using a simple estimate:

$$\begin{gathered} v_i(r,t) = \frac{\dot{R}(t)}{R(t)} r, \quad n_i(r,t) = \frac{n_{i0} R^3(0)}{R^3(t)}\left[1 - \frac{r^2}{R^2(t)}\right]^{3/2}, \\ R(t) = \sqrt{R^2(0) + v_s^2 t^2}, \quad T_{eh} > \frac{ZeQ}{R(0)} \end{gathered} \tag{5}$$

for thermal expansion and

$$\begin{gathered} R(\xi) = R(0)\cosh^2\xi, \quad t(\xi) = \sqrt{\frac{m_i R^3(0)}{8ZeQ}}(\xi + 0.5\sinh(2\xi)), \\ \xi \in [0;\infty], \quad T_{eh} < \frac{ZeQ}{R(0)} \end{gathered} \tag{6}$$

for the Coulomb expansion of a uniformly charged ball. Thus, an increase in E_{las} and τ_{las} together with an increase in H leads to an increase in the rate of cluster expansion and the rate of magnetic field degradation.

There arises an issue about the applicability of concepts (5), (6) about the nature of the motion of cluster ions at high ($a \sim 100$) laser intensities, about the role of ponderomotive pressure of the laser pulse and

a strong magnetic field in this motion, and about the transfer of rotation from electrons to ions. To this end, we performed 3D PIC simulation (EPOCH code [16]) of the expansion of Au^{+30} clusters with a radius from 50 to 300 nm, irradiated by a 10-fs circularly polarized laser pulse with an intensity in the range of 1×10^{19}–5×10^{22} W /cm^2 and propagating along the x axis. The initial concentration of cluster ions, $n_i = 6 \times 10^{22}$ cm^{-3}, corresponded to the certified solid-state density of gold, and the initial concentration of electrons was $Z = 30$ times higher. The initial concentration profile was super-Gaussian of the 4th order; i.e., the cluster boundaries were quite sharp. The laser pulse intensity on the cluster surface reached its maximum at $t = 17.5$ fs. The cluster was located in the center of the simulation box ($x = y = z = 0$). A box measuring $3 \times 3 \times 3$ μm was divided into $800 \times 400 \times 400$ cells along the x, y, and z axes, respectively; the maximum number of particles in a cell was 200 for electrons and 40 for ions. The boundary conditions corresponded to the free exit of particles and radiation from the box, while the transverse size of the laser beam exceeded the size of the box. The software implementation of the code relied on the Villasenor–Buneman current weighting scheme and boundary conditions of a convolutional perfectly matched layer (CPML) [17, 18], which implies compensation of the electric charge, and the quasi-neutrality of the simulation box was not violated.

Calculations have shown that at relatively low intensities, the cluster retains a spherical shape during expansion, its density monotonically decreases from the center to the periphery, and the rate of expansion corresponds to formula (5) or (6) depending on the ratio between T_{eh} and $ZeQ/R(0)$; in this case, the terms corresponding to the ponderomotive pressure force and the Lorentz force on the right-hand side of (3) are small. At an intensity above 10^{21} W/cm^2, the monotonic distribution of the concentration of cluster ions is violated (Fig. 1). Figure 1a shows the spiral structure n_i in the transverse yz plane of the cluster, the formation of which is caused by the rotation of the electric field of the laser wave and the corresponding rotation of the normal component of the ambipolar field on the cluster surface (consistent with the linear Mie theory [12]), shown in Fig. 2. Note that in a homogeneous low-density (transparent) plasma irradiated by a circularly polarized wave of ultrarelativistic intensity, a spiral structure of the ion concentration was also observed [19, 20]. As in the case we are considering, the physical reason for the formation of a spiral structure in a low-density plasma is the rotation of electrons (in our case, a bunch of electrons) in the field of a circularly polarized wave and the ambipolar interaction between electrons and ions.

As was shown in [6], the rotating field extracts part of the electrons of the cluster from its surface and twists them into a spiral. Thus, in addition to the spherically symmetric electron cloud surrounding the ion core, an electron bunch appears at the periphery of the cluster, the impact of which is taken into account on the right-hand side of Eq. (3). It can be shown [14] that the term $\delta n_{bunch}(r)\exp[-(\alpha - \omega t)^2/\delta\alpha^2]$ on the right-hand side of (3) leads to a perturbation of the ion concentration in the form of a spiral structure (see Fig. 1). A comparison of Figs. 1a and 1c shows that the spiral structure expands over time, the outer boundary of the ions expands spherically symmetrically, and its law of motion $R(t)$ is described by formulas (5) and (6). Note that at the end of the laser pulse, the electron bunch rotating around the ion scattering zone occupies a certain angular position: $\delta n_{bunch}(r)\exp[-(\alpha - \omega\tau_{las})^2/\delta\alpha^2]$. The presence of an electron bunch leads to the appearance of an azimuthal force component

$$F_\alpha = (\alpha - \omega\tau_{las})T_{eh}\frac{\delta n_{bunch}(r)}{r}\exp\left[-\frac{(\alpha - \omega\tau_{las})^2}{\partial\alpha^2}\right],$$

which has a different sign for $\alpha > \omega\tau_{las}$ and $\alpha < \omega\tau_{las}$; as a result, the ions in the expansion zone begin to move in opposite directions from the stopping point $\alpha = \omega\tau_{las}$, and the phase diagram of such ions contains regions of azimuthal velocities of different signs [14].

In the longitudinal xz plane (Fig. 1b) one can see a distortion of the spherical shape of the cluster due to the effect of ponderomotive pressure of the laser pulse on the front (irradiated) part of the cluster. Electrons under the action of a circularly polarized wave of a laser pulse are pushed relative to ions at a distance $\delta R_e = a(\lambda/\pi)(n_{cr}/n_e)$ [13], where $\lambda = 2\pi c/\omega$ is the laser wavelength, and $n_{cr} = m_e\omega^2/(4\pi e^2)$ is the critical concentration. Due to the ambipolar field between the shifted electrons and ions, the ions begin to move along the x axis. Estimating the scale of the gradient $\partial/\partial r_x$ as $\partial/\partial r_x \approx 1/\delta R_e$, from Eq. (3) we can obtain an estimate of the velocity v_{ix} and displacement $\delta R_i \approx \int v_{ix}dt$ of ions over time t:

$$\delta R_i \approx \frac{E_{las}^2(2-\eta)t^2}{8\pi m_i n_i \delta R_e} = \frac{ZeE_{las}(2-\eta)t^2}{4m_i} = \frac{2-\eta}{8\pi}\frac{Zm_e}{m_i}\lambda a(\omega t)^2. \quad (7)$$

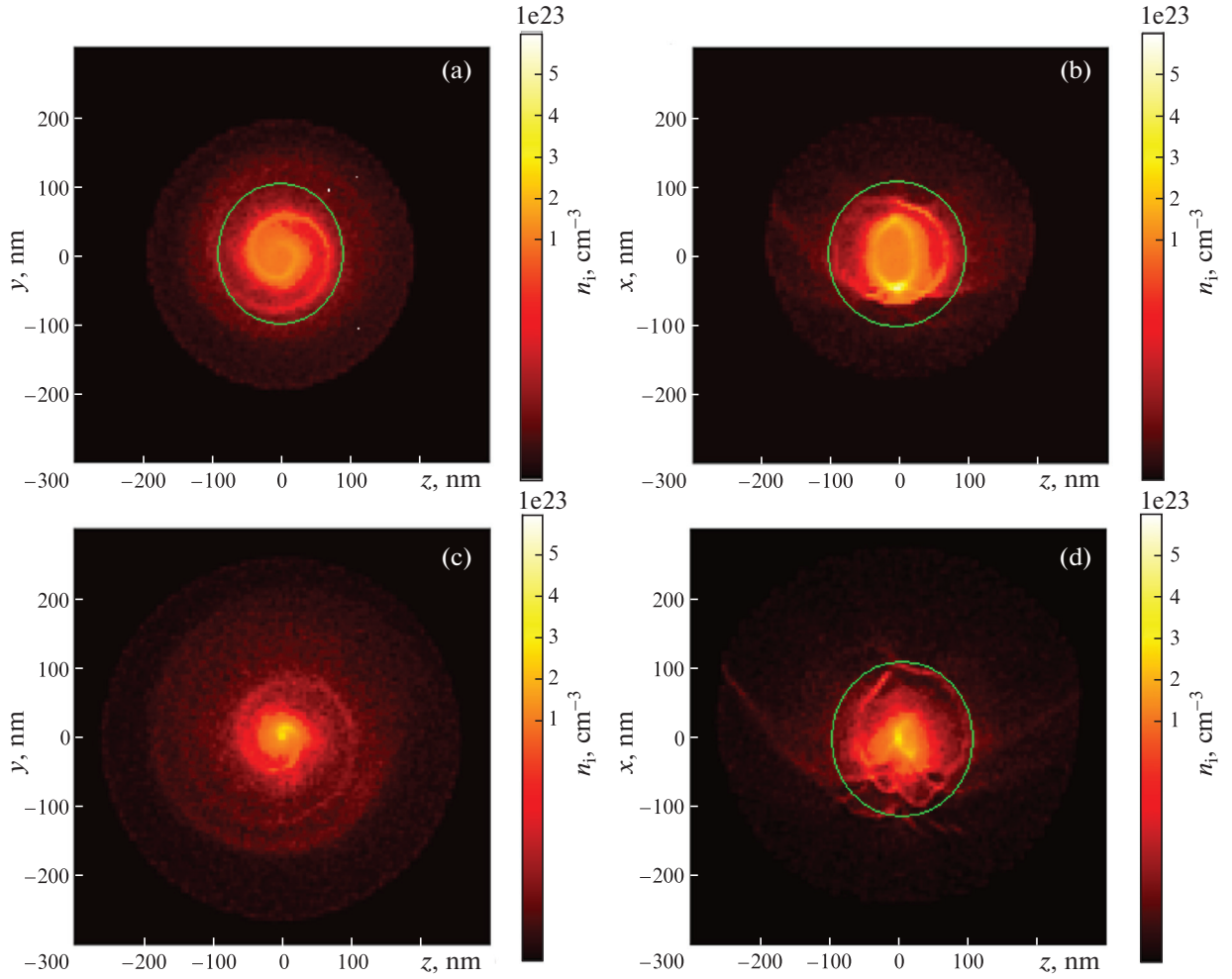

Fig. 1. Ion concentration distributions (a) in the transverse (yz) section ($x = 0$) of an Au^{+30} cluster with $R = 100$ nm at $I_{las} = 10^{22}$ W/cm^2 and $\tau_{las} = 10$ fs; (b) in the longitudinal (xz) section ($y = 0$) at $t = 17.5$ fs, which corresponds to the maximum pulse intensity; and (c, d) at the moment of maximum magnetic field, $t = 27$ fs, with the same parameters. The circle (shown in green) corresponds to the initial radius of the cluster.

At the moment of maximum pulse intensity, we obtain $\delta R_i \sim 30$ nm, which corresponds in Fig. 1b to the distance from the initial cluster boundary (green circle in Fig. 1b) to the n_i boundary in the lower part of the cluster. Chaotic density inhomogeneities in the lower part of the cluster (Fig. 1d) stem from the development of instability due to the applied high pressure of the laser pulse.

In the cylindrical coordinate system $\rho = \sqrt{y^2 + z^2}$ and $\alpha = \arctan(-y/z)$, the spiral equation in Fig. 1a is written as $\rho(\alpha, x, t) = (\alpha v t/2\pi + \rho_0)\sqrt{1 - x^2/R^2}$. A decrease in the effective pitch of the spiral with increasing x (the factor $\sqrt{1 - x^2/R^2}$) is associated with the spherical shape of the cluster, and an increase in the pitch of the spiral with time is associated with the expansion of the cluster. The parameters of the functional dependence $\rho(\alpha, x, t)$ are determined from Figs. 1a and 1c at $x = 0$ and $t = 17.5$ and 27 fs as $v \approx 3$ nm/fs $\sim v_s$ and $\rho_0 \approx 20$ nm, and the value of the ion concentration at the spiral point $y = 0$ and $z = 80$ nm in Fig. 1a as $n_i(x = 0, y = 0, z = 80\text{ nm}) \approx 8 \times 10^{22}$ cm^{-3} on the color scale. In Fig. 1b, the same point with the same value of n_i falls in the region shown as a yellow arc. The equation of this arc $|z| = (vt^* + \rho_0)\sqrt{1 - x^2/R^2}$, $\alpha = 2\pi$ ($t^* = 17$ fs) corresponds to an elliptical arc. Thus, modulation of the cluster density in the form of two elliptical arcs ($\alpha = 0, 2\pi$; $y = 0$ in the spiral equation) in Fig. 1b is associated with the spiral structure inside a spherical cluster and represents its cross section by the zx plane.

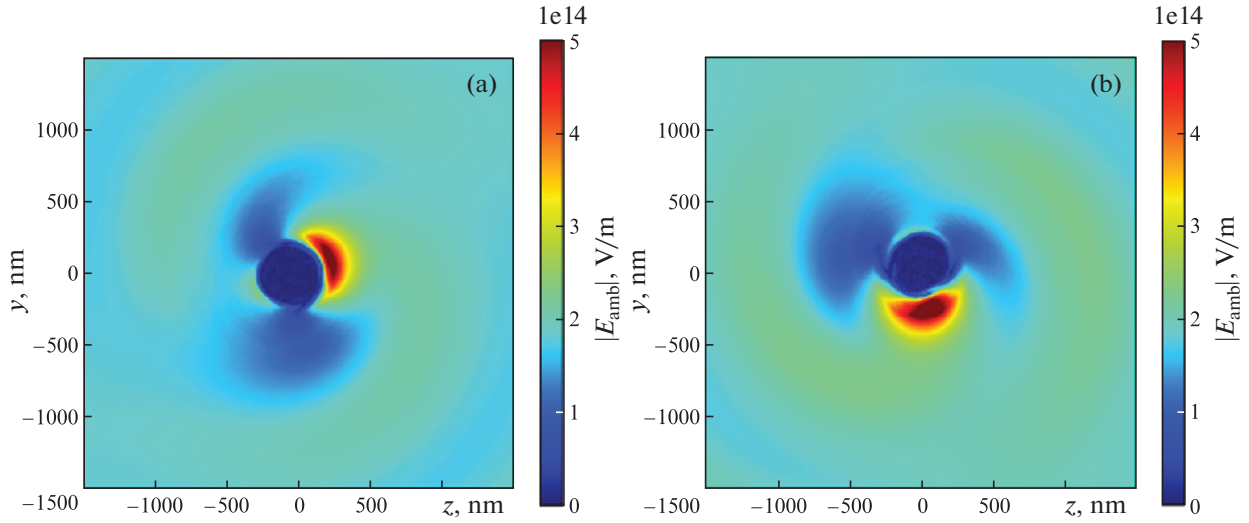

Fig. 2. Rotation of the modulus of the normal component of the electric field on the surface of the cluster in the diametrical plane yz at time instants t = (a) 15 and (b) 17.5 fs (laser pulse maximum). Here the coordinate x = 60 nm (cluster center at x = 0) corresponds to the position where, according to Mie theory, the field maximum should be. The dark blue circle (low field) with a radius of 200 nm corresponds to field screening in the inner region of the cluster.

It was shown in [8] that the characteristic radius of electron orbits is from three to four R. Accordingly, the optimal duration of a laser pulse for isotropic expansion (5) should not exceed $\tau_{\text{las max}} \approx 4R/v_s$. Substituting $\tau_{\text{las max}}$ into (1), we obtain the maximum possible magnetic field of the cluster for a given laser intensity:

$$\frac{eH_{\max}}{m_e\omega c} = a_H \approx \frac{\eta a^{3/2}}{(1+a^2)^{1/2}}\sqrt{\frac{m_i}{Zm_e}}. \tag{8}$$

According to (8), magnetic fields are possible that exceed the initial laser field: $a_H > a$. Formula (8) also shows an increase in $H_{\max}$ with increasing a ($\sim a^{1/2}$), and so it is advisable to limit ourselves to the currently available experimental range of laser intensities (no higher than 10^{22} W/cm^2). Note that the dependence $\eta = \eta(a, R)$ is possible, and then the scaling $H_{\max} \sim a^{1/2}$ may change. The estimate $\tau_{\text{las max}} \approx 4R/v_s$ implies the absence of a Coulomb explosion, for which the field of the ion core of the cluster must be greater than the laser field:

$$\frac{4\pi}{3}Zen_iR\left(\frac{e}{m_e\omega c}\right) > E_{\text{las}}\left(\frac{e}{m_e\omega c}\right).$$

Accordingly, to implement $H_{\max}$ we need a cluster of size

$$R > R_{\min}(I) \approx \frac{3am_ec\omega}{4\pi Ze^2n_i}. \tag{9}$$

Thus, the dependence of $H_{\max}$ on the cluster radius at other fixed parameters has a local maximum: clusters of small radius are not able to hold electrons, and at large radii the field decreases with increasing radius in accordance with (1). For the same reasons, the dependence of $H_{\max}$ on laser intensity at other fixed parameters also has a local maximum. The results of 3D PIC calculations (Fig. 3) confirm the existence of an optimal intensity for the selected radius and an optimal radius for the selected intensity. One can see from Fig. 3 that the strongest magnetic field that was obtained by optimizing the parameters reaches 15 GG for a cluster with a radius of 200 nm and a laser intensity of 10^{22} W/cm^2. This value corresponds to the estimate from formula (8) for the absorption coefficient $\eta \approx 0.2$. The spatial distribution of the magnetic field corresponds to the dipole field and is given in our previous works [6, 7].

Let us analyze the results of the numerical calculation in more detail in order to find the deviation of the ion dynamics from the isotropic expansion model. In a 15 GG magnetic field, the ions in the central region of the cluster (where, according to (5), their velocity v_i is less than the velocity v_s at the periphery)

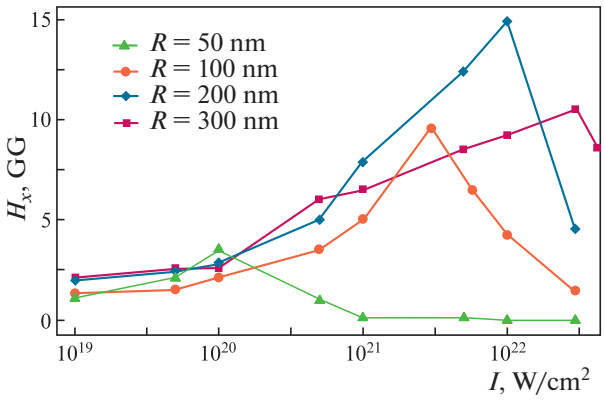

Fig. 3. Maximum amplitude of the magnetic field of the Au^{+30} cluster ($t = 27$ fs) as a function of the laser intensity and cluster radius. The laser pulse duration $\tau_{las} = 10$ fs.

are magnetized, and their Larmor radius is less than the distance to the cluster boundary. In this case, in the equation of ion motion (3), the magnetic component of the Lorentz force becomes significant, and the transverse expansion should slow down. To confirm this, let us consider the spatial distribution of the ion concentration for a cluster of optimal radius at an optimal laser intensity and a maximum magnetic field (Fig. 4). One can see that the cluster ions in the process of interaction are divided into two zones—the expansion zone (shown in black and gray) and the compression zone (red and yellow). One can also see the stage of the compression zone formation in Figs. 1b and 1d at a smaller cluster radius and a smaller magnetic field. The ion concentration in the compression zone in Fig. 4 significantly exceeds the initial concentration of 6×10^{22} cm^{-3}, in contrast to Fig. 1, where the degree of compression is lower. The behavior of ions in the expansion zone during the entire interaction with the pulse corresponds to the above-described analytical model, and the motion of ions in the compression zone does not correspond to formulas (5) and (6). The division of ions into two zones is associated with their velocity distribution [see (5)], when the ions of the central region of the cluster have a gyroradius less than the radius of the cluster itself. The transverse expansion of such ions is slower relative to ions in the peripheral region, which have a higher radial velocity. The electrons of the cluster are also divided into two regions, and the ambipolar field acting between the ions and electrons leads to the radial expansion of the inner and outer ionic regions with different velocities. The division of ions into two zones and the movement of the boundaries of these zones at different velocities are clearly visible in the phase diagrams of the ions shown in Fig. 5.

Figures 5b and 5c show the transverse expansion of the outer zone, the velocity of which reaches $\sim 0.1c$, and the expansion from the compression zone with a significantly lower maximum velocity, about $0.02c$. The main part of the ions in the compression zone has a velocity of $\sim 0.01c$ and is magnetized according to the estimate of the ion gyroradius. The characteristic radius of the compression zone in Figs. 4 and 5 is approximately 50 nm, which corresponds to the gyroradius $R_H = v_i/\Omega$ of an ion with a velocity $v_{iy,z} \sim 0.01c$ in the compression region (Figs. 5b and 5c). The outer radius of the cluster in Figs. 5b and 5c, equal to ~ 500 nm, corresponds to formula (5). The concentration of ions (longitudinally elongated) in the compression zone (Fig. 4) is estimated as $n_{i0}(R(0)/R_H)^2 \approx 6 \times 10^{22}\ (200/50)^2$ cm$^{-3} \approx 10^{24}$ cm^{-3}. Note that the azimuthal component of the ambipolar force is less than the radial one, since $n_{0e}(r) \gg \delta n_{bunch}$, and $v_{i\alpha}/v_{i\rho} \sim 0.01$ for ions in the expansion region. In the compression zone, ions rotate only in one direction, and $v_{i\alpha}/v_{i\rho} \sim 1$.

The estimate of the maximum possible magnetic field (8) is based on an estimate of the cluster lifetime $\tau_{las\,max} \approx 4R/v_s$. Obtaining long-lived magnetic fields requires reducing the expansion velocity, which will happen if the ions become magnetized (the ion gyroradius becomes less than the cluster radius). The presence of an ion compression zone changes the temporal dynamics of the magnetic field (2). Figure 6 shows the dependence of the magnetic field modulus on time (the spatial region of effective localization of the magnetic field has a radius of ~ 200 nm). This dependence exhibits characteristic behavior that differs from the time dependence at a lower magnetic field [8]. The maximum magnetic field value of 15 GG (the first peak in Fig. 6), achieved after the laser pulse leaves the simulation box, is approximately twice the electric field of the pulse, which is consistent with estimate (8) for $\eta \approx 0.2$. However, Fig. 6 shows a second time peak, which is not described by formula (2) that is absent in [7, 9] due to lower values of the magnetic field.

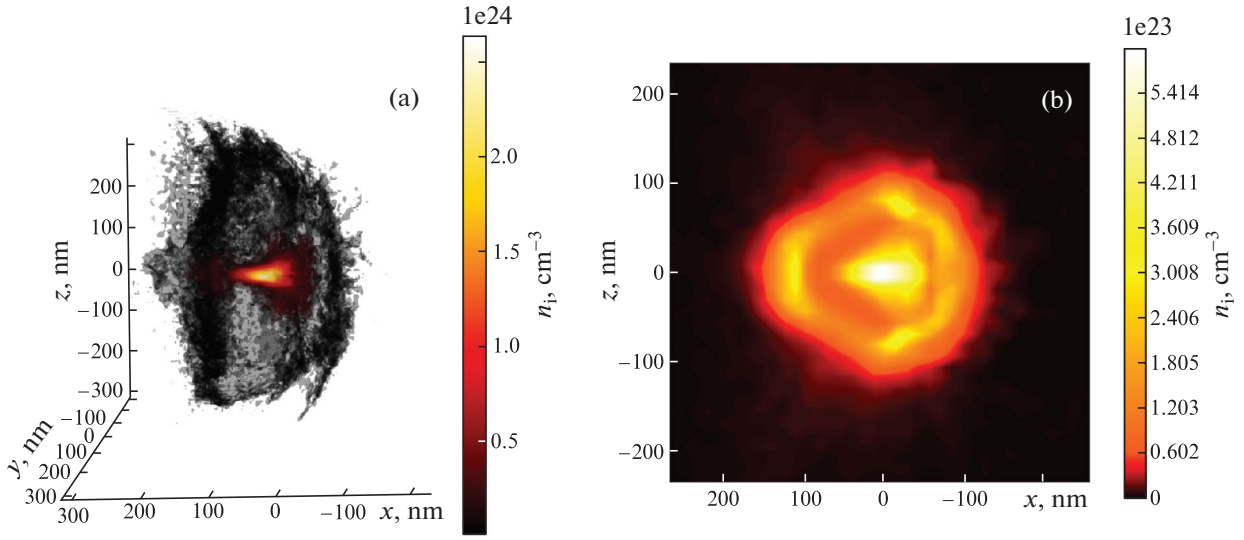

Fig. 4. (a) 3D distribution of ion concentration in the volume of the simulation box at the moment of a maximum magnetic field ($t = 27$ fs) and (b) its cross section by the $y = 0$ plane. The cluster radius $R(0) = 200$ nm, $I_{las} = 10^{22}$ W/cm^2, and $\tau_{las} = 10$ fs. Regions of low concentration n_i are not shown on the scale.

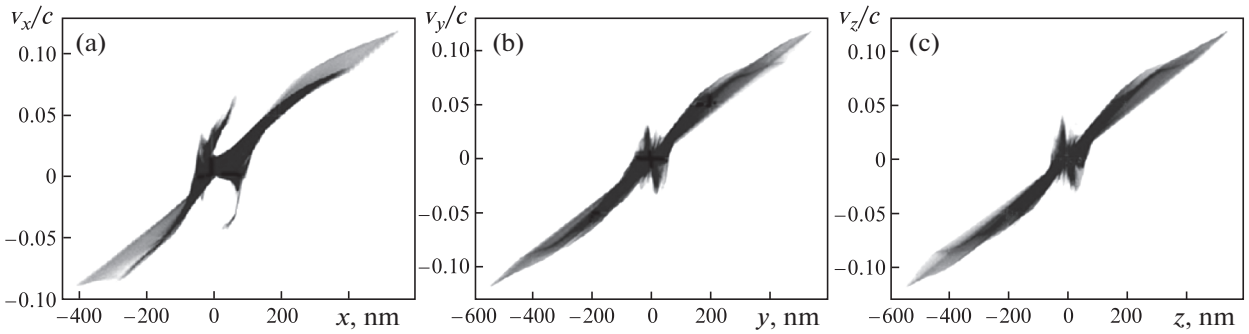

Fig. 5. Phase diagrams of ions along Cartesian axes at the moment of a maximum magnetic field modulus ($t = 27$ fs) at $R = 200$ nm, $\tau_{las} = 10$ fs and $I_{las} = 10^{22}$ W/cm^2.

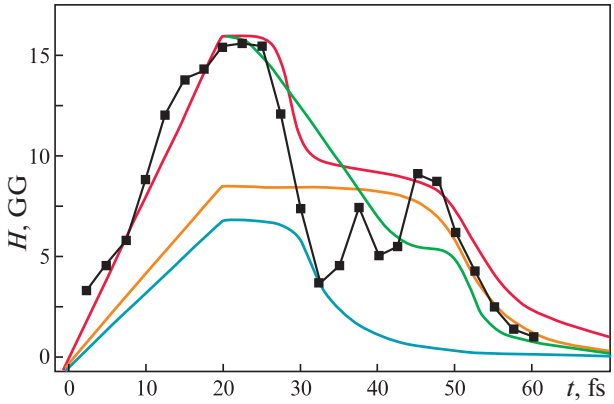

Fig. 6. Time dependence of the magnetic field modulus of a cluster with radius $R = 200$ nm upon interaction with a pulse of intensity $I_{las} = 10^{22}$ W/cm^2 and duration $\tau_{las} = 10$ fs [the black curve shows the numerical calculation; blue, thermal expansion model $H_{out}(t)$; orange, thermal expansion model $H_{in}(t)$; red, total model field $H(t)$ in the case of thermal expansion; green, total model field $H(t)$ in the case of Coulomb expansion with cluster charges $Q_{in} = 90$ pC and $Q_{out} = 70$ pC].

The presence of the second peak is associated with the appearance of a significant part of the magnetized ions (compression zone). The compression zone expands at a lower speed, and its lifetime exceeds the $R(0)/v_s$ estimate, since the magnetic field in the compression zone retains ions, which in turn slow down the rate of decrease in the magnetic field. Thus, the increased lifetime of the magnetic field in Fig. 6 is explained by the presence of a dense magnetized region in the center of the cluster with a lower expansion velocity.

For analytical estimates of the amplitude and lifetime of the magnetized region field, we use system (3), (4) in the time interval after the laser pulse termination ($t \in [t_{\max}; \infty]$, where $t_{\max}$ is the moment of the laser pulse termination and the magnetic field maximum). In this case, the system (at $\delta n_{\text{bunch}} < n_{0e}$) describes the adiabatic expansion of a bunch of hot plasma in a strong magnetic field. The rate of transverse expansion here is greatly slowed down, since the radial component of the thermal pressure force of hot electrons in (3) is compensated by the radial component of the Lorentz force. Anisimov and Lysikov [10] showed that in this case, there is a self-similar solution to system (3), (4), in which the ion concentration $n_i(\mathbf{r}, t)$ is described by a triaxial ellipsoid with semi-axes $X(t)$, $Y(t)$ and $Z(t)$ varying over time. The time dependence of the functions $X(t)$, $Y(t)$, and $Z(t)$ is determined by the system of equations of motion of an effective "particle" with coordinates $X(t)$, $Y(t)$, and $Z(t)$ in the potential $U(X, Y, Z)$ and magnetic field:

$$\ddot{Y} + \Omega\dot{Z} = -\frac{\partial U}{\partial Y}, \quad \ddot{Z} - \Omega\dot{Y} = -\frac{\partial U}{\partial Z}, \quad \ddot{X} = -\frac{\partial U}{\partial X},$$
$$U = \frac{(5\chi - 3)u_s^2}{\chi - 1}\left[\frac{X(t_{\max})[Y^2(t_{\max}) + Z^2(t_{\max})]}{X(t)[Y^2(t) + Z^2(t)]}\right]^{\chi - 1}, \tag{10}$$

where

$$\Omega(t) = \Omega(t_{\max})\frac{X(t_{\max})[Y^2(t_{\max}) + Z^2(t_{\max})]}{X(t)[Y^2(t) + Z^2(t)]};$$
$$\chi = 5/3; \quad t \in [t_{\max}; \infty];$$

and $m_i u_s^2$ is the initial (at $t_{\max}$) thermal energy of the ion.

The type of solution to system (10) is determined by the ratio of the parameters $u_s/\Omega(t_{\max})$ (ion gyroradius) and $[Y^2(t_{\max}) + Z^2(t_{\max})]^{1/2} = R_\perp(t_{\max})$. For $u_s/[\Omega R_\perp(t_{\max})] \gg 1$ we have a spherically symmetric solution $[X^2(t) + Y^2(t) + Z^2(t)]^{1/2} = R(t)$, the ion density $n_i(\mathbf{r}, t)$ and $R(t)$ for which are given in formula (5). In the opposite limiting case, $u_s/[\Omega R_\perp(t_{\max})] \ll 1$, the ions are magnetized, their transverse (yz) expansion is slowed down, and the density ellipsoid is strongly elongated along the x axis. Equations (10) describe the adiabatic thermal expansion of a cluster in a magnetic field.

In the case of Coulomb expansion in a magnetic field in system (10), the form of potential energy changes:

$$U_Q(X, Y, Z) \sim \frac{ZeQ}{\sqrt{X^2 - R_\perp^2}} \ln\frac{X + \sqrt{X^2 - R_\perp^2}}{X - \sqrt{X^2 - R_\perp^2}}. \tag{11}$$

At $R_\perp \to X$, the electrostatic potential of the ellipsoid (11) turns into the potential of a charged ball: $U_Q \sim ZeQ/\sqrt{X^2 + R_\perp^2}$.

Note that system of equations (10) follows from the Lagrange function,

$$L = \frac{\dot{X}^2 + \dot{Y}^2 + \dot{Z}^2}{2} + \frac{\Omega(t)}{2}(\dot{Y}Z - \dot{Z}Y) - U(X, Y, Z) \tag{12}$$

of an effective "particle" with coordinates $X(t)$, $Y(t)$, and $Z(t)$. In the transverse (Y, Z) plane, the Lagrange function (12) with potential (11), due to the axial symmetry of the potential, has an integral of motion—angular momentum—and an integral of energy. However, the equations of motion for the semi-axis $X(t)$ and the transverse radius $R_\perp(t) = [Y^2(t) + Z^2(t)]^{1/2}$ turn out to be related, and their joint analytical solution is impossible.

To explain the calculation results presented in Fig. 6, we solve system (10) as follows. In accordance with Figs. 4 and 5, we divide the region occupied by ions into two spatial regions (two ellipsoids). We denote the parameters of the ellipsoids by the corresponding subscripts: $X_{\text{in, out}}(t)$, $Y_{\text{in, out}}(t)$, $Z_{\text{in, out}}(t)$,

$R_{\perp \text{in, out}}(t)$, $R_{\text{in, out}}(t)$, $u_{s\text{in, out}}$, and $n_{\text{iin, out}}$. The outer ellipsoid has the following initial parameters: radius $R_{\text{out}}(t_{\max}) = R = 200$ nm, and $X_{\text{out}}(t_{\max}) = Y_{\text{out}}(t_{\max}) = Z_{\text{out}}(t_{\max})$. The inner ellipsoid has the following initial parameters: radius $R_{\perp\text{in}}(t_{\max}) = 50$ nm, $Y_{\text{in}}(t_{\max}) = Z_{\text{in}}(t_{\max})$, and $X_{\text{in}}(t_{\max}) = R$. As the initial ion velocities (in accordance with Fig. 6), we use $u_{s\text{out}} = 0.1c$ and $u_{s\text{in}} = 0.01c$. Note that $u_{s\text{out}} \approx v_s$, and $u_{s\text{in}}$ corresponds to the condition of magnetization of the inner ellipsoid, i.e., the condition of equality of magnetic and thermal pressures [21]: $m_i n_{\text{iin}} u_{s\text{in}}^2 \approx H^2(t_{\max})/8\pi$, whence $u_{s\ \text{in}} \approx H(t_{\max})/\sqrt{8\pi m_i n_{\text{iin}}}$. The initial value $R_{\perp\text{in}}(t_{\max})$ corresponds to the gyroradius of the ion: $R_{\perp\text{in}}(t_{\max}) = u_{s\ \text{in}}/\Omega(t_{\max})$.The maximum value of the magnetic field $H(t_{\max}) = 15$ GG will be distributed between the zones in proportion to the number of electrons and ions in each zone (since the zones are approximately quasi-neutral): $H(t_{\max}) = H_{\text{out}}(t_{\max}) + H_{\text{in}}(t_{\max})$, where $H_{\text{out}}(t_{\max}) = 4$ GG and $H_{\text{in}}(t_{\max}) = 11$ GG. Time evolution of ellipsoid fields has the form:

$$H_{\text{out}}(t) = H_{\text{out}}(t_{\max})\frac{R_{\text{out}}^3(t_{\max})}{X_{\text{out}}(t)R_{\perp\text{out}}^2(t)},$$

$$H_{\text{in}}(t) = H_{\text{in}}(t_{\max})\frac{X_{\text{in}}(t_{\max})R_{\perp\text{in}}^2(t_{\max})}{X_{\text{in}}(t)R_{\perp\text{in}}^2(t)}.$$

Considering the total magnetic field of the cluster to be the sum of the fields of two ellipsoids, we obtain

$$H(t) = H_{\text{out}}(t_{\max})\frac{R_{\text{out}}^3(t_{\max})}{X_{\text{out}}(t)R_{\perp\text{out}}^2(t)} + H_{\text{in}}(t_{\max})\frac{X_{\text{in}}(t_{\max})R_{\perp\text{in}}^2(t_{\max})}{X_{\text{in}}(t)R_{\perp\text{in}}^2(t)}. \tag{13}$$

In order to construct the time evolution of the field over the entire time interval $t \in [0; \infty]$, we will assume that according to (1) the magnetic field of each of the ellipsoids increases linearly in time over the interval $t \in [0; t_{\max}]$. Thus, using (13), it is possible to construct a model dependence of $H(t)$ and compare it with numerical simulation data (Fig. 6). Note that independent consideration of the expansion of each of the ellipsoids is an approximation that does not correspond to the condition of continuity of the solution of system (3), (4) at the interface between the ellipsoids. The presented model also neglects the mutual influence of the ellipsoids through the general magnetic field of the external ellipsoid, which is acceptable for $H_{\text{out}}(t) < H_{\text{in}}(t)$. The justification for the approximations made is the correspondence (within a factor on the order of unity) of the hydrodynamic expansion velocities of the inner and outer ellipsoids to the phase diagrams (Fig. 5) obtained by numerical PIC simulation.

Let us present a numerical (MCAD) solution to Eqs. (10) for each of the ellipsoids with the initial conditions described above in the case of thermal expansion regime. In Fig. 6, the blue curve shows the field $H_{\text{out}}(t)$; the orange curve, $H_{\text{in}}(t)$; and the red curve, $H(t)$. One can see that the model of two ellipsoids flying apart according to (10) explains an increase in the lifetime of the magnetized region and the behavior of the $H(t)$ curve during the thermal mechanism of cluster expansion.

To estimate the characteristic decay times of the blue and orange curves in Fig. 6 in the form of analytical formulas relating these times to the parameters of the laser pulse and cluster, we present following considerations. The outer ellipsoid expands almost isotropically according to law (5) with $u_{s\ \text{out}} \approx v_s$ and $R_{\text{out}}(t_{\max}) \approx R$, and the characteristic decay time of the blue curve is $\tau_{\text{out}} \sim 4R/v_s$. In the transverse ($Y_{\text{in}}$, Z_{in}) plane of the inner ellipsoid, the equations of motion (10) of the effective "particle" can be solved analytically under the assumption that $X_{\text{in}}(t) \equiv 0$ (this estimate is accurate to a factor on the order of unity). The law of expansion in the transverse direction, $R_{\text{in}\perp}(t) = \sqrt{Y_{\text{in}}^2(t) + Z_{\text{in}}^2(t)}$, at $X_{\text{in}}(t) \equiv 0$ is determined by the integral

$$t = \int\limits_{R_{\text{in}}(t_{\max})}^{R_{\perp\text{in}}} d\rho \left\{ \frac{2}{m_i}[U(X_{\text{in}} = 0, R_{\perp\text{in}}(t_{\max})) - U(X_{\text{in}} = 0, R_{\perp\text{in}}(t))] - \frac{\Omega_{\text{in}}^2(t_{\max})R_{\perp\text{in}}^4(t_{\max})}{4\rho^2}\left(1 - \frac{R_{\perp\text{in}}^2(t_{\max})}{\rho^2}\right)^2 \right\}^{-1/2}. \tag{14}$$

Along the direction of the magnetic field, the law of expansion of the inner ellipsoid is also determined by formula (14), but in this case $\Omega_{\text{in}}(t_{\max}) = 0$. Accordingly, for the expansion of the inner ellip-

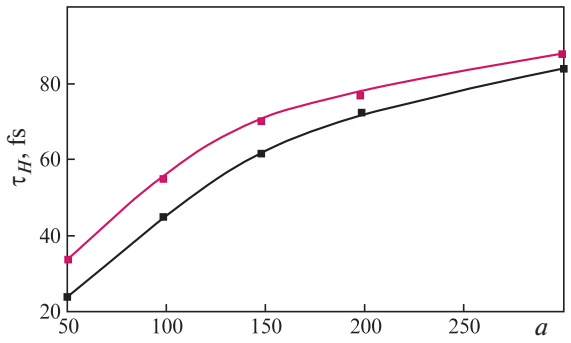

Fig. 7. Dependences of the magnetic field lifetime τ_H on the dimensionless amplitude a of the laser pulse for an Au^{+30} cluster with a radius of 200 nm at a laser pulse duration τ_{las} = (black curve) 10 and (red curve) 15 fs.

soid in the transverse direction compared to the expansion in the longitudinal direction, the delay time Δt will be

$$\Delta t = \int\limits_{R_{in}(t_{max})}^{\infty} d\rho \left\{ \frac{2}{m_i}[U(X_{in} = 0, R_{\perp in}(t_{max})) - U(X_{in} = 0, R_{\perp in}(t))] \right.$$
$$\left. - \frac{\Omega_{in}^2(t_{max}) R_{\perp in}^4(t_{max})}{4\rho^2}\left(1 - \frac{R_{\perp in}^2(t_{max})}{\rho^2}\right)^2 \right\}^{-1/2} - \int\limits_{R_{in}(t_{max})}^{\infty} d\rho \qquad (15)$$
$$\times \left\{ \left\{ \frac{2}{m_i}[U(X_{in} = 0, R_{\perp in}(t_{max})) - U(X_{in} = 0, R_{\perp in}(t))] \right\}^{-1/2} \right.$$

Obviously, $\Delta t \to 0$ at $\Omega \to 0$. The characteristic decay time of the orange and red curves according to (15) is estimated as

$$\tau_H = \tau_{out} + \Delta t. \qquad (16)$$

Calculation using formula (16) yields $\tau_{in} \approx 43$ fs, which corresponds to the PIC simulation. Since the parameters $\Omega(t_{max})$, $R_{\perp in}(t_{max})$ and $u_{s\,in}$, which determine the values of the integrals in (15), have the above estimates in terms of the cluster and laser pulse parameters, we can construct the $\tau_H(a, \tau_{las}, R)$ dependences. Figure 7 shows the $\tau_H(a)$ dependences for an Au^{+30} cluster with a radius of 200 nm at a laser pulse duration $\tau_{las} = 10$ fs (black curve) and $\tau_{las} = 15$ fs (red curve).

It can be shown that under the Coulomb mechanism of cluster expansion, with an appropriate choice of parameters, the time evolution of the magnetic field will be determined by two relaxation times and the time dependence of the field will be similar to that shown in Fig. 6. To do this, as in the case of thermal expansion, we divide the region occupied by ions into two spatial regions (two ellipsoids) with charges Q_{in} and Q_{out} and the initial lengths of the semi-axes given above. The outer ellipsoid expands isotropically according to law (6) with parameters Q_{out}, $R_{out}(t_{max}) \approx R$. The semi-axis $X_{in}(t)$ of the inner ellipsoid (along the magnetic field), up to a factor on the order of unity, also increases according to law (6) at Q_{in}, $X_{in}(t_{max}) \approx R$. The law of transverse expansion (14) with the replacement $U \to U_Q$ allows one to find $R_{\perp in}(t)$ and construct, using formula (13), the time evolution of the magnetic field of a cluster under the Coulomb mechanism of its expansion. In Fig. 6, the green curve for $Q_{in} = 90$ pC and $Q_{out} = 70$ pC (the charge ratio coincides with the ratio of the numbers of ions in each of the ellipsoids, $Q_{in}/Q_{out} = N_{in}/N_{out}$, and the total charge corresponds to the removal of 4% of the cluster electrons) shows the time dependence of $H(t)$ (13) in the case of the Coulomb expansion mechanism. It can be seen that it also exhibits an increased magnetic field lifetime.

Thus, the dynamics of ions and the magnetic field as a result of the interaction of a cluster with a circularly polarized pulse can be described as follows. During the action of a laser pulse, the ions are separated into approximately two regions as a result of the combined action of the ponderomotive force from the incident pulse and the Lorentz force from the generated magnetic field. The magnetic field and density of the ion compression region reach their maximum by the end of the laser pulse. After this, the second stage of ion dynamics begins, which corresponds to the decay of the outer zone in accordance with the

model of isotropic thermal and Coulomb expansion of the plasma ball and the decay of the inner zone at a rate several times lower than the decay rate of the outer zone. The time dependence of the magnetic field according to ion dynamics has two peaks corresponding to the emergence and decay of each of the ion regions.

4. CONCLUSIONS

We have considered some new aspects of the motion of ions and the temporal dynamics of the magnetic field in a laser cluster plasma. It has been shown that intense circularly polarized laser radiation leads to the appearance of a spiral structure of the ion density in the cluster volume. The strong quasi-stationary magnetic field arising from the rotation of electrons causes a spatial separation of the ions into approximately two zones: the internal compression zone and the external expansion zone. The inner zone has an increased density compared to the initial zone and an increased lifetime compared to the outer zone. Ion dynamics turns out to be interconnected with the dynamics of the magnetic field. In addition to the increased lifetime, the time dependence of the magnetic field has a characteristic two-peak appearance associated with the emergence and decay of each of the spatial ion bands.

FUNDING

The work was supported by the Russian Science Foundation (grant no. 23-22-00110); calculations were performed on the computer cluster of the Peter the Great St. Petersburg Polytechnic University.

CONFLICT OF INTEREST

The authors of this work declare that they have no conflicts of interest.

REFERENCES

1. Krainov, V.P. and Smirnov, M.B., *Phys. Usp.,* 2000, vol. 43, p. 901.
2. Smirnov, M.B. and Krainov, V.P., *Laser Phys.,* 2003, vol. 13, p. 490.
3. Fennel, Th., Meiwes-Broer, K.-H., Tiggesbäumker, J., Reinhard, P.-G., Dinh, P.M., and Suraud, E., *Rev. Mod. Phys.,* 2010, vol. 82, p. 1793.
4. Gozhev, D.A., Bochkarev, S.G., and Bychenkov, V.Yu., *JETP Lett.,* 2021, vol. 114, no. 4, p. 200.
5. Frolov, A.A., *Plasma Phys. Rep.,* 2018, vol. 44, p. 40.
6. Lecz, Zs. and Andreev, A., *Phys. Rev. Res.,* 2020, vol. 2, p. 023088.
7. Andreev, A.A., Platonov, K.Yu., Lecz, Zs., and Hafz, N., *Sci. Rep.,* 2021, vol. 11, p. 15971.
8. Andreev, A.A. and Platonov, K.Yu., *Quantum Electron.,* 2021, vol. 51, no. 5, p. 446.
9. Lécz, Z., Konoplev, I.V., Seryi, A., and Andreev, A., *Sci. Rep.,* 2016, vol. 6, p. 36139.
10. Anisimov, S. and Lysikov, Yu., *J. Appl. Math. Mech.,* 1970, vol. 34, p. 882.
11. Braenzel, J., Andreev, A.A., Ehrentraut, L., Sandner, W., Schnürer, M., Platonov, K., and Klingsporn, M., *Phys. Rev. Lett.,* 2015, vol. 114, no. 12, p. 124801.
12. Andreev, A.A. and Litvinov, L.A., *Opt. Spectrosc.,* 2023, vol. 131, p. 252.
13. Gibbon, P., *Short Pulse Laser Interactions with Matter: An Introduction,* Imperial College Press, 2005. https://doi.org/10.1142/P116
14. Platonov, K.Yu., Lecz, Zs., and Andreev, A.A., in *Proc. 20th Int. Conf. Laser Optics (ICLO 2022), St. Petersburg, Russia,* 2022, p. 235.
15. Bychenkov, V.Yu. and Kovalev V.F., *Plasma Phys. Rep.,* 2005, vol. 31, no. 2, p. 178.
16. Particle-in-cell code for plasma physics simulations. https://github.com/Warwick-Plasma/epoch.
17. Villasenor, J. and Buneman, O., *Comput. Phys. Commun.,* 1992, vol. 69, p. 306. https://doi.org/10.1016/0010-4655(92)90169-Y
18. Roden, A.J. and Gedney, S., *Microwave Opt. Technol. Lett.,* 2000, vol. 27, p. 334.
19. Bulanov, S.V., Esirkepov, T.Zh., Califano, F., Kato, Y., Liseykina, T.V., Mima, K., Naumova, N.M., Nishihara, K., Pegoraro, F., Ruhl, H., Sentoku, Y., and Ueshima, Y., *JETP Lett.,* 2000, vol. 71, no. 10, p. 407. https://doi.org/10.1134/1.568365
20. Sharma, A., *Sci. Rep.,* 2018, vol. 8, p. 2191. https://doi.org/10.1038/s41598-018-20506-x
21. Akhiezer, A.I., *Elektrodinamika plazmy* (Electrodynamics of Plasma), Moscow: Nauka, 1974.

Translated by I. Ulitkin